Environmental Pollution 341 (2024) 122874

Contents lists available at ScienceDirect

Environmental Pollution

journal homepage: www.elsevier.com/locate/envpol

Nickel oxide nanoparticles induce cell wall modifications, root anatomical changes, and nitrosative signaling in ecotypes of Ni hyperaccumulator *Odontarrhena lesbiaca*☆

Selahattin Kondak [a,b,*], Patrick Janovszky [c], Réka Szőllősi [a], Árpád Molnár [a], Dóra Oláh [a,b], Oluwatosin Peace Adedokun [a], Panayiotis G. Dimitrakopoulos [d], Andrea Rónavári [e], Zoltán Kónya [e], László Erdei [a], Gábor Galbács [c], Zsuzsanna Kolbert [a]

[a] Department of Plant Biology, University of Szeged, Közép fasor 52., 6726, Szeged, Hungary
[b] Doctoral School of Biology, Faculty of Science and Informatics, University of Szeged, Közép fasor 52., 6726, Szeged, Hungary
[c] Department of Inorganic, Organic and Analytical Chemistry, University of Szeged, Dóm tér 7-8., 6720, Szeged, Hungary
[d] Department of Environment, University of the Aegean, 81100, Mytilene, Greece
[e] Department of Applied and Environmental Chemistry, University of Szeged, Rerrich Béla tér 1., 6720, Szeged, Hungary

ARTICLE INFO

Keywords:
Ampeliko
Ecotypes
Loutra
Nanoparticles
Nickel oxide
Nitrosative signaling
Alyssum lesbiacum
Olympos

ABSTRACT

The industrial application and environmental release of nickel oxide NPs (NiO NPs) is increasing, but the details of their relationship with plants are largely unknown. In this work, the cellular, tissue, organ, and molecular level responses of three ecotypes of Ni hyperaccumulator *Odontarrhena lesbiaca* grown in the presence of high doses of NiO NP (250 mg/L and 500 mg/L) were studied. All three ecotypes showed a similar accumulation of Ni in the presence of nano Ni, and in the case of NiO NPs, the root-to-shoot Ni translocation was slighter compared to the bulk Ni. In all three ecotypes, the walls of the root cells effectively prevented internalization of NiO NPs, providing cellular defense against Ni overload. Exposure to NiO NP led to an increase in cortex thickness and the deposition of lignin-suberin and pectin in roots, serving as a tissue-level defense mechanism against excessive Ni. Exposure to NiO NP did not modify or cause a reduction in some biomass parameters of the Ampeliko and Loutra ecotypes, while it increased all parameters in Olympos. The free salt form of Ni exerted more negative effects on biomass production than the nanoform, and the observed effects of NiO NPs can be attributed to the release of Ni ions. Nitric oxide and peroxynitrite levels were modified by NiO NPs in an ecotype-dependent manner. The changes in the abundance and activity of *S*-nitrosoglutathione reductase protein triggered by NiO NPs suggest that the enzyme is regulated by NiO NPs at the post-translational level. The NiO NPs slightly intensified protein tyrosine nitration, and the slight differences between the ecotypes were correlated with their biomass production in the presence of NiO NPs. Overall, the *Odontarrhena lesbiaca* ecotypes exhibited tolerance to NiO NPs at the cellular, tissue, organ/organism and molecular levels, demonstrating various defense mechanisms and changes in the metabolism of reactive nitrogen species metabolism and nitrosative protein modification.

1. Introduction

Nickel (Ni) is a geogenic element and also an essential micronutrient for plants. It plays a crucial role in the activity of urease, hydrogenase, and Ni-superoxide dismutase (Mustafa et al., 2023). Additionally, Ni has been found to induce the glyoxalase enzyme and regulate the cellular glutathione pool, thus contributing to the beneficial role of Ni in plants (Fabiano et al., 2015). In soils, the average concentration of Ni does not exceed 100 mg/kg (Shahzad et al., 2018). Due to its widespread use in various manufacturing processes (e.g., stainless steel and heat-resisting steel production), the environmental concentration of Ni has been increased (Hussain et al., 2013). Furthermore, the use of nickel oxide nanoparticles (NiO NP) is becoming more common in heavy industries and consumer products, particularly in the smelting, iron and steel,

☆ This paper has been recommended for acceptance by Dr Parvaiz Ahmad.

* Corresponding author. Department of Plant Biology, University of Szeged, Közép fasor 52., 6726, Szeged, Hungary.
E-mail address: kondaksela@bio.u-szeged.hu (S. Kondak).

https://doi.org/10.1016/j.envpol.2023.122874
Received 12 July 2023; Received in revised form 22 September 2023; Accepted 3 November 2023
Available online 8 November 2023

coinage, and electrical goods industries (Danjumma et al., 2019; Manna et al., 2021). The nanoforms of Ni have special physicochemical properties that include high surface area, specific optical, magnetic, electrical properties, increased stability, hardness, and antimicrobial effects (Kolbert et al., 2022). As a result of their increasing production and utilization, the chances of NiO NPs entering the environment and contacting plants are increasing.

As sessile organisms, most plants are negatively affected by elevated concentrations of soil Ni, since excess absorption of Ni can disrupt metabolic processes, leading to inhibition of enzyme activity, chlorophyll biosynthesis, and photosynthetic electron transport (Sreekanth et al., 2013; Genchi et al., 2020). The unique properties of Ni nanoforms influence their interaction with plants most of which experience various microscopic (e.g., chromosomal aberrations, cell cycle perturbations, Manna et al., 2022) and macroscopic (e.g., chlorosis, necrosis, growth inhibition, wilting, Lin and Xing, 2007; Stampoulis et al., 2009) injuries.

Furthermore, Ni is known to reduce cell wall plasticity (Shi and Cai, 2009), induces modifications in the chemical composition of the cell wall (Kolbert et al., 2020) and the toxicity of Ni is often associated with its negative effect on ion balance and disruption of membrane functionality (Saad et al., 2016). Membrane stability can be compromised by the overproduction of reactive oxygen species (ROS) (Halliwell and Gutteridge, 1984) and excess Ni induces the formation of ROS (including hydrogen peroxide, H_2O_2 and hydroxyl radical) and causes oxidative stress; however, due to its redox-inactive nature, in an indirect way (Gajewska et al., 2006; Khaliq et al., 2015; Khair et al., 2020; Kumar et al., 2022; Bhat et al., 2023).

Although Ni-induced imbalance of ROS homeostasis has been revealed in a number of plant species, little is known about the effect of excess Ni on the metabolism of reactive nitrogen species (RNS) (Kolbert et al., 2020). Nitric oxide (NO) and the nonradical species *S*-nitrosoglutathione (GSNO) and peroxynitrite ($ONOO^-$) are the biologically relevant members of RNS (Molassiotis and Fotopoulos, 2011). In biological systems, glutathione reacts with NO to form *S*-nitrosoglutathione (GSNO), which is a more stable and less reactive molecule than NO. GSNO can release NO and propagate the NO signal over long distances through the xylem. The GSNO reductase enzyme (GSNOR) reduces GSNO and produces glutathione disulphide and ammonia, thus controlling the intracellular level of GSNO, therefore, it is an important regulator of NO signaling (Jahnová et al., 2019). Nitric oxide and other RNS regulate physiological processes through post-translational modifications such as protein tyrosine nitration, which is a specific modification of tyrosine residues that alters protein structure and function (Kolbert et al., 2017; Corpas et al., 2021). Covalent addition of a nitro group to specific tyrosines of proteins can generally induce loss or sometimes gain of function, and also no obvious effect on protein function is possible (Kolbert et al., 2017). Protein tyrosine nitration may also alter other signal transduction pathways by preventing tyrosine phosphorylation (Galetskiy et al., 2011).

The described negative effects of Ni occur in non-accumulator plants, but Ni hyperaccumulators possess special metal metabolism that enables them to colonize high Ni-containing serpentine soils without showing toxicity symptoms. Serpentine soils can contain several thousand mg/kg Ni (Hseu and Chen, 2019) and this special type of soil is not optimal for most plant species, also because they have a granular-rocky texture and low water retention capacity (Kruckeberg, 2002). Additionally, such soils can be characterized by suboptimal concentration levels of phosphorus, nitrogen and potassium, and a supraoptimal amount of heavy metals such as manganese, cobalt, chromium, or nickel (Hseu and Chen, 2019). Hyperaccumulator plants do not only grow in the presence of high Ni concentrations, but also have the ability to accumulate more than 1000 mg/kg Ni in their shoots (Reeves, 1992). Compared to non-accumulators, nickel hyperaccumulators exhibit increased uptake, root-to-shoot translocation, and capacity for detoxification and sequestration of nickel (Rascio and Navari-Izzo, 2011; Hipfinger et al., 2022). Hyperaccumulators absorb nickel primarily as Ni^{2+} which is then transported from the roots to the shoots as citrate, malate, or histidine complexes (Ingle et al., 2005). Of the 532 Ni hyperaccumulators, 62 species belong to the genus *Odontarrhena* (syn. *Alyssum,* Brassicaceae) (Reeves et al., 2017), and most of them grow on serpentine soils of southeast Europe and in the Middle East (Reeves et al., 2021). An endemic species growing on serpentine soils in Lesbos, Greece, is *Odontarrhena lesbiaca* (previously *Alyssum lesbiacum),* which is a perennial plant of maximum 40 cm tall (Strid and Tan, 2002; Kazakou et al., 2010). Previously, it was revealed that populations of *O. lesbiaca* derived from different locations have a different hyperaccumulation capacity of Ni (Adamidis et al., 2014), which is related to the amount of Ni in the soil in the original habitat (Kazakou et al., 2010). The present study examines three *Odontarrhena* ecotypes (Ampeliko, Loutra, and Olympos), the comparison of which was motivated by the fact that the effects of NiO NPs on these Ni hyperaccumulator species have not yet been characterized with particular attention paid to Ni accumulation, microelement homeostasis, changes in root structure, and nitro-oxidative processes.

2. Materials and Methods

2.1. Characterization of NiO NPs

NiO nanoparticles were obtained from Sigma-Aldrich (St. Louis, USA, catalog number: 637130). The particle size, chemical composition, and crystallinity of the nanoparticles were investigated using transmission electron microscopy (TEM) images and electron diffraction (ED) patterns captured by a FEI Tecnai G2 20 X-Twin instrument (FEI Corporate Headquarters, Hillsboro, OR, USA) with an acceleration voltage of 200 kV. X-ray diffraction (XRD) was also performed using Cu Kα radiation on a Rigaku MiniFlex II powder diffractometer (Rigaku Corporation, Tokyo, Japan) to verify the composition of the particles by cross-referencing their crystallinity with the literature. The scanning rate was $2°min^{-1}$ over a 2θ range of 5°–80°. Energy dispersive X-ray spectroscopy (EDS) was applied to estimate the elemental analysis of the sample. The EDS measurement was carried out on a Hitachi S-4700 scanning electron microscope (30 kV accelerating voltage) equipped with a Röntec energy dispersive X-ray spectrometer. The specific surface area of the samples was calculated by the 5-point Brunauer-Emmett-Teller (BET) method from N_2 adsorption isotherms recorded at 77.15 K on a Quantachrome NOVA 3000e instrument (Quantachrome, FL, USA). Samples were degassed for 1.5 h at 373.15 K before measurement.

2.2. Preparation of treatment liquids

For the nano-sample, NiO NPs were dispersed in distilled water, resulting in a heterogeneous suspension containing large NiO NP aggregates, which was then dispersed using an ultrasound sonicator for 2 times 30 min. The pH of the suspension was adjusted to 5.7–5.8 and the final concentration was set at 250 mg/L or 500 mg/L NiO NP. For the bulk sample, a sufficient amount of $NiCl_2 \times 6H_2O$ was dissolved in distilled water and the pH was adjusted to 5.7–5.8, with volume adjusted to achieve a final concentration of 250 mg/L or 500 mg/L $NiCl_2$.

2.3. Plant-growing conditions

The seeds of *Odontarrhena lesbiaca* were collected from more than 100 randomly selected individuals grown at three geographically distinct serpentine sites located on Lesbos Island, Greece. Ampeliko, Olympos, and Loutra (site details are described in Kazakou et al., 2010). The seeds collected were surface sterilized with 70% (v/v) ethanol for 1 min, followed by a treatment with 5% (v/v) sodium hypochlorite for 15 min, and then placed in Petri dishes filled with filter paper moistened with distilled water (control) or an equal volume of aqueous solutions of $NiCl_2$ or NiO NP suspension. The Petri dishes were kept in a greenhouse

for 5 days under controlled conditions (photon flux density of 150 μmol m^{-2} s^{-1}), 12/12 h light and dark cycle, a relative humidity of 45–55% and a temperature of 25 ± 2 °C. All analyses were performed using 5-days-old seedlings.

2.4. Analysis of Ni concentration by ICP-MS

The roots and shoots of the *Odontarrhena lesbiaca* ecotypes were collected separately and dried at 70 °C for 24 h 100 mg of dried plant material was incubated with 6 ml of trace analytical quality nitric acid (65% w/v, Reanal, Hungary) for 2 h, followed by the addition of 2 ml of hydrogen peroxide (30% w/v, VWR Chemicals, Hungary). The samples were then subjected to microwave-assisted digestion at 200 °C and 1600 W for 2 h in closed PTFE reaction vessels (MarsXpress CEM, Matthews, USA). The analysis of the nickel content of the resulting solutions was performed on a quadrupole Agilent 7700X (Santa Clara, USA) inductively coupled plasma mass spectrometer (ICP-MS) equipped with the standard Agilent integrated sample introduction system. The instrumental parameters used were the following: 1550 W plasma forward power, 15.0 L/min plasma gas flow rate, 1.05 L/min carrier gas flow rate, 10.0 mm plasma sampling depth, 1 s integration time and 600 μL/min sample uptake rate. Determinations were made by recording signals at the ^{60}Ni isotope, using ^{45}Sc as internal standard to correct for potential matrix effects and helium collision cell technology to eliminate polyatomic interferences (He cell gas flow rate: 5 ml/min, octopole bias: 18 V, energy discrimination: 5 V). Instrumental tuning was performed before all measurements using Agilent's tuning solutions (No. G1820-60410). The built-in Agilent Mass Hunter software was used for data evaluation.

2.5. Laser-induced breakdown spectroscopy (LIBS)

Prior to the measurements, the plantlets were carefully removed from the Petri dishes and their roots were rinsed with trace analytical quality laboratory water to clean them from the cultivation medium. The seedlings were then pressed, dried, and mounted on a glass microscope slide with a thin layer of epoxy regime (Epoxy-Embedding Kit, 45359, Sigma-Aldrich, Germany). LIBS spectra were taken using a J-200 LA-LIBS tandem spectrometer (Applied Spectra Inc., USA) in the LIBS mode, using the following settings: laser wavelength 266 nm, laser pulse duration 6 ns, laser pulse energy 14 mJ, spot size 60 μm, integration time 1.05 ms, gate delay 0.5 μs, laser pulse repetition rate 10 Hz. The sample translation speed and direction were set to allow a stepwise scanning over an area encompassing the entire plantlets (ca. 15–20 × 50–60 mm) with no overlapping measurement points, and from each location single-shot LIBS spectra were recorded. The recorded spectrum from each analytical spot consisted of a data vector with over 12,000 pixels, representing the UV–Vis optical emission spectrum over the wavelength range of 190–1040 nm with an optical resolution of 0.07 nm. From each plant, multiple layers were ablated in order to ablate the whole plant sample; then the spectra were summed in each location vertically; thus, we gained enough spectral data from the samples to continue with the data evaluation and the creation of the elemental maps. Evaluation of the hyperspectral data set was performed using Clarity software (Applied Spectra Inc., USA), whereas elemental maps were visualized using ImageLab software (Epina GmbH, Austria). Nickel elemental maps were created on the basis of net signal intensities measured at the Ni I 352.4 nm spectral line.

2.6. TEM analysis of the root and hypocotyl sections

Samples from the mature zone of the root and hypocotyl were fixed with 3% glutardialdehyde in PBS (pH 7.4), embedded in Embed812 (EMS, Hatfield, PA, USA), and prepared as 70 nm thin sections using an Ultracut S ultramicrotome (Leica, Vienna, Austria). Sections were then stained with uranyl acetate and lead citrate and observed under a Jeol 1400 plus transmission electron microscope (Jeol, Tokyo, Japan) according to Molnár et al. (2020).

2.7. Observing root anatomy and cell wall components (lignin, suberin, pectin) in root tissues

Observations on root anatomy were made under a Zeiss Axiovert 200 M microscope (Carl Zeiss, Jena, Germany).

Cross sections of roots were prepared similarly to those prepared by Barroso et al. (2006). The mature root pieces were fixed in a 4% (w/v) paraformaldehyde solution and then washed with distilled water. They were then embedded in 5% (w/v) bacterial agar following a slightly modified version of the method described by Zelko et al. (2012). The embedded samples were cut into 100 μm thick root cross sections using a vibratome (Zeiss-Microm, HM650V). To visualize lignin plus suberin in the root cross sections, Auramine-O staining was used. Cross sections were stained in a dye solution (0.01% (w/v) prepared in 10 mM Tris-HCl buffer, pH 7.4) for 10 min in the dark. (Rahoui et al., 2017). To obtain bright field microscopic images, a different set of root cross sections was stained with 0.02% (w/v) toluidine blue (TB) for 1 min at room temperature under light (Mitra and Loqué, 2014).

Ruthenium Red (RR) was used to visualize the pectin content of the root tips, following the method described by Durand et al. (2009). Roots were incubated in 0.05% (w/v) RR solution for 15 min, washed with distilled water and placed on slides.

2.8. Evaluating biomass production

The primary root length and the shoot length were measured manually and expressed in centimeters (cm). Fresh weight of the root and shoot (FW) and dry weight (DW, after drying the plant material at 70 °C for 24 h) were measured using an analytical balance and expressed in milligrams (mg).

2.9. Determination of RNS levels in roots

The nitric oxide (NO) content of the root tips was analyzed with 4-amino-5-methylamino 2′,7′-difluorofluorescein diacetate (DAF-FM DA). Samples were stained for 30 min in fluorophore solution (10 μM, prepared in 10 mM Tris-HCl buffer, pH 7.4), washed two times with the buffer solution, and placed on slides (Kolbert et al., 2012).

Dihidrorhodamine 123 (DHR) was used for the detection of peroxynitrite ($ONOO^-$) levels according to Kolbert et al. (2012). Samples were stained with 10 μM DHR 123 solution (in 5 mM Tris-HCl buffer, pH 7.4), incubated for 15 min at room temperature and washed twice with the buffer solution before microscopic analysis.

2.10. Fluorescence and light microscopy

All analyses were performed using an Axiovert 200 M invert fluorescence microscope (Carl Zeiss, Jena, Germany). Filter set 10 (exc: 450–490, em: 515–565 nm) was used for the DAF-FM, DHR, and Auramine-O measurements. Pixel intensity was measured in the area of circles. The circles' radii were set to cover the largest sample area. Axiovision Rel. 4.8 software (Carl Zeiss, Jena, Germany) was applied to measure pixel intensity on digital photographs.

2.11. Analysis of GSNOR activity by UV–vis absorption spectroscopy

The plant material (250 mg of shoot and root separately) was ground with a double volume of extraction buffer consisting of 50 mM Tris - HCl buffer (pH 7.6–7.8), 0.1 mM EDTA, 0.1% Triton X-100 and 10% glycerol and GSNOR activity was measured by observing NADH oxidation in the presence of GSNO at 340 nm, following the method described by Sakamoto et al. (2002). The plant homogenate was centrifuged at 9300×*g* for 20 min at 4 °C, and 150 μL of protein extract was incubated

in a 1 mL reaction buffer containing 20 mM Tris–HCl pH 8.0, 0.5 mM EDTA, 0.2 mM NADH and 0.4 mM GSNO. The data are expressed as nanomoles of NADH/min/mg protein, and protein concentration was measured using the Bradford protein assay (1976). Measurements were performed using a Kontron Uvikon double-beam UV–vis absorption spectrometer spectrophotometer.

2.12. Protein extraction and analysis of GSNOR protein abundance and tyrosine nitration by western blot

The shoot and root of the ecotypes of *Odontarrhena lesbiaca* were ground with a double volume of extraction buffer consisting of 50 mM Tris - HCl buffer (pH 7.6–7.8), 0.1 mM EDTA, 0.1% Triton X-100 and 10% glycerol. The resulting mixture was centrifuged at 9300×*g* for 20 min at 4 °C. The protein extract was treated with a 1% protease inhibitor cocktail and stored at −20 °C. Protein concentration was determined using bovine serum albumin as a standard according to Bradford (1976).

After denaturation with SDS PAGE (12%), 15 μg of protein extract was subjected to wet blotting (25 mA, 16 h). The resulting membranes were used for cross-reactivity assays with different antibodies. The loading controls were performed using an anti-actin antibody (Agrisera, Cat. No. AS13 2640), and actin (bovine muscle, Sigma-Aldrich, cat No. A3653) was used as protein standard. GSNOR immunoassays were conducted with a polyclonal primary antibody obtained from rabbit (anti-GSNOR, Agrisera, cat. No. AS09 647) and an affinity-isolated goat anti-rabbit IgG–alkaline phosphatase secondary antibody (Sigma-Aldrich, cat. No. A3687, 1:10,000, see details in Oláh et al., 2020). For the detection of protein tyrosine nitration, anti-3-nitrotyrosine (Sigma-Aldrich, cat. No. N0409, diluted 1:2000) was used as the primary antibody. Secondary antibody was the same as before. The visualization of the bands was accomplished using the NBT/BCIP (5-bromo-4--chloro-3-indolylphosphate) reaction. For the purpose of a positive control, nitrated bovine serum albumin (NO_2-BSA) obtained from Sigma-Aldrich (cat. No. A3653) was used. The quantification of protein bands was performed using Gelquant software (biochemlabsolutions.com) and expressed as pixel densities. Western blot analysis was performed on three separate protein extracts obtained from independent plant generations, and each extract was subjected to the process at least two times (Kolbert et al., 2018).

2.13. Statistical analysis

All results are shown as mean values of raw data (±SD). For statistical analysis, Duncan's multiple range test (OneWay ANOVA, $P < 0.05$) was used in SigmaPlot 12. For ANOVA assumptions, we used Hartley's Fmax test for homogeneity and the Shapiro-Wilk test for normality.

3. Results and discussion

3.1. Physicochemical characteristics of NiO NPs

The NiO nanoparticles were visualized by TEM, which illustrated that the particles have rhombus and rod-shaped shapes (Figs. S1 and A). Based on the image analysis, the average particle size was found to be 23.2 ± 8.3 nm. The ED (Figs. S1 and A inset) and XRD results (Figs. S1 and B) verified the crystallinity and chemical composition of the particles. The characteristic reflections are at 2θ values of 37.2°, 43.3°, 62.8°, 75.3° and 79.3°, characteristic of nickel oxide with cubic crystalline structure (Mateos et al., 2019). EDS measurement was carried out to estimate the elemental composition of the sample (Figs. S1 and C). It can be clearly seen that the sample contained Ni and O and was free of other elements, indicating a material with a high degree of purity. The specific surface area was calculated with the BET equation; the NiO sample has a specific surface area of 76.40 m^2/g, which is in the typical range of similar NiO materials (Wang et al., 2006).

3.2. Exposure to NiO NP causes milder Ni accumulation compared to bulk Ni in the shoot of Odontarrhena seedlings

Treatment with NiO NP caused a concentration-dependent increase in the Ni content of the roots of the ecotypes (Table 1). In the case of Ampeliko, 2.9 and 7.2 times the accumulation of Ni compared to the control were induced by 250 and 500 mg/L of NiO NP treatments, respectively. A similar trend was observed for the Loutra and Olympos ecotypes. It should be noted that exposure to 250 mg/L NiO NP caused only a 1.2-fold increase in Ni content in Olympos roots, while in Ampeliko and Loutra it was 2.8 and 2.7 times, respectively. In comparison, 250 mg/L $NiCl_2$ caused higher accumulation of Ni in the roots than NiO NP at the same concentration. This is particularly evident in the Olympos ecotype, where 250 mg/L $NiCl_2$ treatment resulted in a 4.64 times higher Ni concentration in the root system than the NiO NP treatment (Table 1).

In the shoot system of untreated *Odontarrhena* ecotypes, notably high Ni contents (4000–6000 μg/g DW) were measured (Table 1), which reflects the Ni hyperaccumulator character of this species. Interestingly, the Ni content in the shoot of all three ecotypes only slightly increased as a result of the NiO NP treatment, which suggests that the majority of the Ni released from the NPs or internalized in NP form remains in the root. The poor root-to-shoot translocation of Ni is supported by the reduction of the translocation factors below the value of 1 in the *Odontarrhena* ecotypes exposed to NiO NP (Table 1). This is in contrast to Ni salt treatment, where shoot Ni content increased dramatically in all three ecotypes, reaching values of 10,000–12,000 μg/g DW (Table 1). The

Table 1
Ni concentrations (μg/g dry weight, DW) in the root and shoot system of the ecotypes of *Odontarrhena lesbiaca* (Ampeliko, Loutra, Olympos) grown in the presence of 0, 250 or 500 mg/L of NiO NP or $NiCl_2 \times 6H_2O$. Translocation factors were calculated (see Materials and methods).

Ecotype/Treatment	root [Ni] μg/g DW	shoot [Ni] μg/g DW	Translocation factor
O. lesbiaca Ampeliko 0 mg/L NiO NP	1052.21 ± 19.11	5592.52 ± 77.18	5.31
O. lesbiaca Ampeliko 250 mg/L NiO NP	3038.12 ± 23.14	5674.29 ± 57.75	1.86
O. lesbiaca Ampeliko 500 mg/L NiO NP	7573.15 ± 56.21	6269.75 ± 88.25	0.82
O. lesbiaca Loutra 0 mg/L NiO NP	948.78 ± 17.22	4428.64 ± 28.34	4.66
O. lesbiaca Loutra 250 mg/L NiO NP	2581.25 ± 9.66	4994.95 ± 21.18	1.93
O. lesbiaca Loutra 500 mg/L NiO NP	9566.24 ± 31.82	5576.49 ± 166.33	0.58
O. lesbiaca Olympos 0 mg/L NiO NP	1186.85 ± 25.60	4538.57 ± 7.39	3.82
O. lesbiaca Olympos 250 mg/L NiO NP	1480.96 ± 19.04	5009.04 ± 117.54	3.38
O. lesbiaca Olympos 500 mg/L NiO NP	8813.02 ± 145.93	5388.61 ± 141.86	0.61
O. lesbiaca Ampeliko 0 mg/L $NiCl_2$	844.12 ± 0.01	6988.41 ± 0.16	8.27
O. lesbiaca Ampeliko 250 mg/L $NiCl_2$	5467.66 ± 0.03	8898.81 ± 0.33	1.62
O. lesbiaca Ampeliko 500 mg/L $NiCl_2$	9069.75 ± 0.09	11601.10 ± 0.11	1.27
O. lesbiaca Loutra 0 mg/L $NiCl_2$	975.36 ± 0.002	5308.93 ± 0.31	5.44
O. lesbiaca Loutra 250 mg/L $NiCl_2$	5185.62 ± 0.03	7093.00 ± 0.26	1.36
O. lesbiaca Loutra 500 mg/L $NiCl_2$	8991.49 ± 0.05	9616.90 ± 0.05	1.06
O. lesbiaca Olympos 0 mg/L $NiCl_2$	1193.24 ± 0.01	6801.26 ± 0.31	5.69
O. lesbiaca Olympos 250 mg/L $NiCl_2$	6923.81 ± 0.06	8432.92 ± 0.06	1.21
O. lesbiaca Olympos 500 mg/L $NiCl_2$	8309.98 ± 0.19	9975.73 ± 0.26	1.20

translocation factors in $NiCl_2$-treated plants remained above the value of 1 indicating that the *Odontarrhena* ecotypes sustained an effective root-to-shoot translocation capacity when exposed to Ni in the bulk salt form. The observed difference in Ni translocation suggests that a part of the NiO NP may be bound in the root cell walls or in the root cells and a smaller amount of Ni ions are released from them and reach the shoot through the xylem, compared to that in the case of Ni salt.

It can be concluded that there are no significant differences between the ecotypes in terms of Ni accumulation as the effect of NiO NPs or the bulk Ni form. At the same time, the rates of root-to-shoot Ni translocation were different, depending on the nano- or ionic form of Ni exposure.

3.3. Distribution of Ni in Odontarrhena seedlings exposed to ionic or nano-Ni

The ICP-MS results were supplemented with LIBS elemental mapping which is capable of detecting the spatial distribution of Ni in plantlets in any chemical form (Limbeck et al., 2021; Galbács, 2022; Janovszky et al., 2023). A higher Ni-specific atomic emission intensity may indicate Ni uptake from both its ionic and NP forms.

In general, the LIBS technique did not detect significant levels of Ni

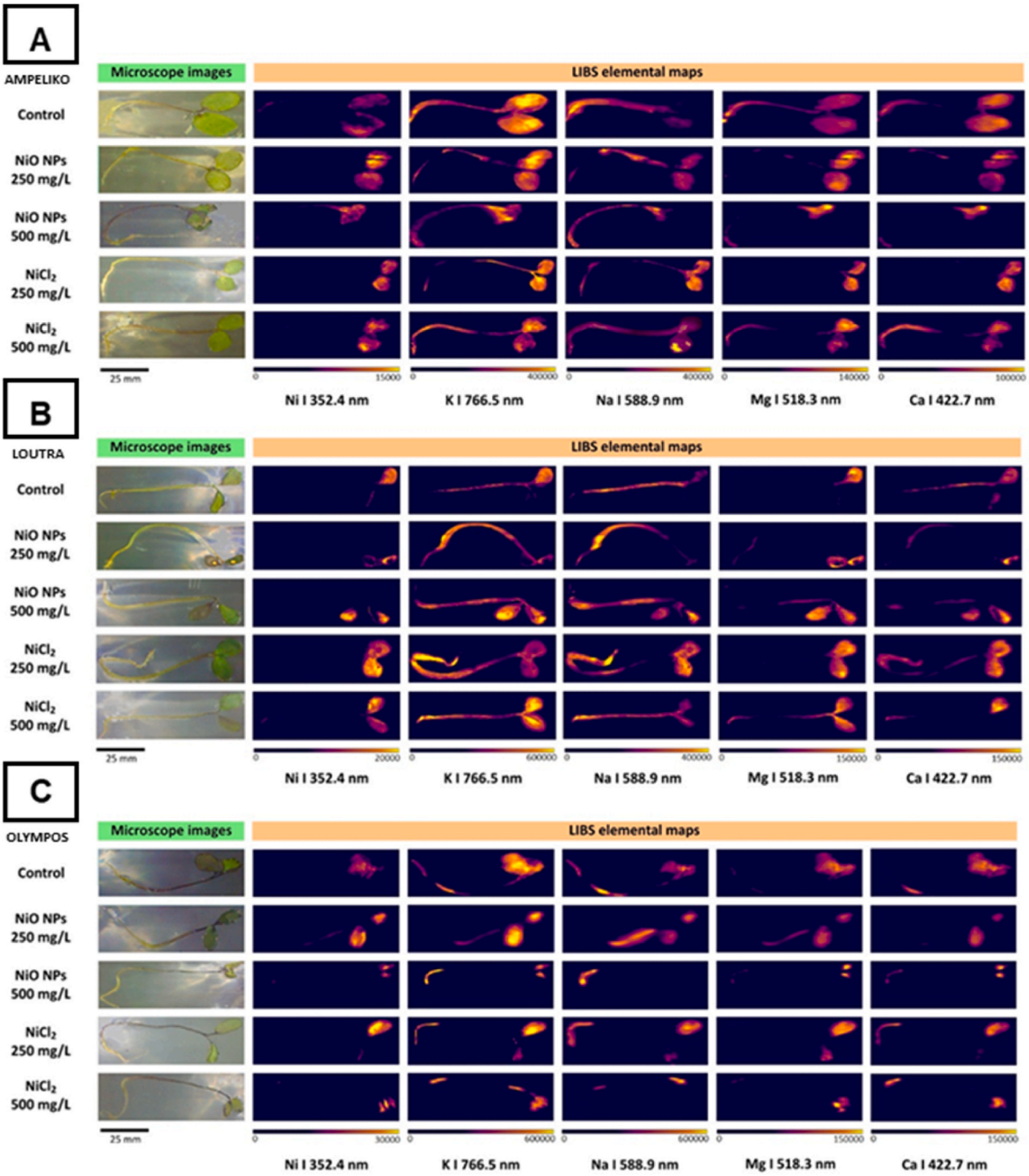

Fig. 1. Representative LIBS elemental maps demonstrating the *in planta* distribution of selected nutrients in the ecotypes of Ampeliko (A), Loutra (B) and Olympos (C) of *Odontarrhena lesbiaca* seedlings cultivated with 0 (Control, Cont), 250 mg/L or 500 mg/L NiO NP or $NiCl_2 \times 6H_2O$ for 5 days. The pixel color scale in the maps shows the net optical emission intensity of the given spectral line of the element, which is proportional with the concentration (e.g. deep blue corresponds to a very low concentration, and light yellow corresponds to a high concentration). (For interpretation of the references to colour in this figure legend, the reader is referred to the Web version of this article.)

in the hypocotyls and roots of *Odontarrhena* seedlings (Fig. 1). In the cotyledons of the Loutra and Olympos ecotypes, the $NiCl_2$-induced Ni signal was more intense than that induced by NiO NP. However, in the Ampeliko ecotype, the NiO and $NiCl_2$-induced signals were similar in intensity, suggesting a difference between ecotypes. On the basis of the signal scale, which is related to the concentration, it appears that NiO-treated Ampeliko contains a larger amount of Ni compared to the other ecotypes. This is supported by the larger area containing Ni in Ampeliko, even though the signal level in Olympos is similar at around 15,000. It should be noted that similar levels of Ni signal were detected at NiO or $NiCl_2$ concentrations, suggesting that in this experimental system LIBS could not indicate concentration-dependent effects in contrast to ICP-MS. Instead of a Ni-specific transporter, root Ni uptake seems to be catalyzed by poorly selective cation transporters (van der Pas and Ingle, 2019), suggesting that increased Ni ion uptake influences absorption of other divalent cations. Therefore, beyond Ni, the distribution of other elements, mainly divalent cations, was visualized in NiO NP or $NiCl_2$-treated *Odontarrhena* seedlings. Mild changes were detected, indicating that the nutrient homeostasis of Ampeliko, Loutra, and Olympos seedlings is stable despite the high Ni load. Furthermore, in the case of some elements (e.g. Na, Mg, Ca), an increase in signal intensity occurred as a result of exposure to Ni. It is conceivable that the activation of the Ni ion transport system promotes the uptake of other (divalent) cations in these hyperaccumulators.

Collectively, the LIBS approach provides spatial information about the distribution of elements, and these results support the hypothesis that LIBS is suitable for the visualization of macroelement and microelement distributions mainly in the shoot of Ni hyperaccumulator seedlings.

3.4. NiO NPs interact with the walls of root cells

The previous data on Ni ion concentration and translocation factors assumed that the nanoparticles could be bounded by the root cell wall. This possibility was examined by TEM, and in the case of NiO NP-treated ecotypes, an increased electron-dense signal was detected in the root the cell wall compared to the untreated control (Fig. 2), suggesting that a significant part of the NPs might be bound. Within the root cells, we did not observe any electron-dense signal considered NiO NPs. Due to the relatively large size of the NPs (Fig. S1), there is a low probability that the NPs enter the cells. However, cellular uptake cannot be completely excluded due to the fact that NPs are capable of increasing the pore size of the cell wall (Kurczyńska et al., 2021; Oliveira et al., 2023). We did not observe an electron-dense signal suspected to be associated with NiO NPs in cells from the lower and upper parts of the hypocotyl (data not shown), from which we conclude that the NP translocation from the root to the shoot was negligible. The TEM results support the ICP-MS data and suggest that the root cell walls bounded a significant part of the NiO NPs, preventing internalization and consequently limiting the NP translocation to the aerial parts.

3.5. NiO NPs induce changes in the structure of the root tissue and the composition of the cell wall of Odontarrhena seedlings

First, we determined the tissue characteristics of the root *Odontarrhena lesbiaca,* choosing the untreated Ampeliko ecotype as a model. In the cross section of the differentiation zone, the following tissues could be distinguished: the rhizodermis, consisting of trichoblast and atrichoblast cells; 2–3 layers of cortical cells; the endodermis showing U-shaped cell wall thickening (tertiary endodermis); the pericycle; and the stele containing two bundles of xylem and two bundles of phloem tissues (diarch stele) (Fig. S2).

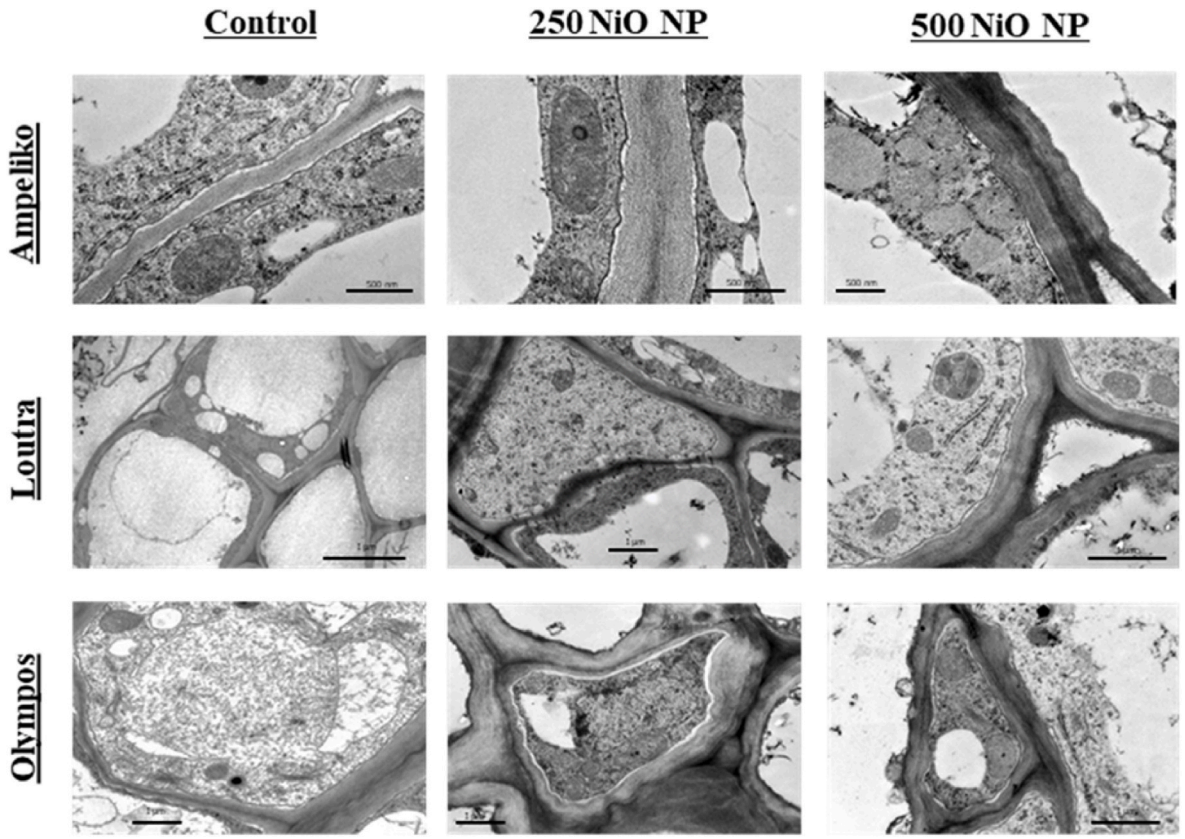

Fig. 2. TEM images showing root cells of the *Odontarrhena lesbiaca* ecotypes (Ampeliko, Loutra Olympos) treated with 0 mg/L (control), 250 mg/L and 500 mg/L NiO NP.

In the roots of the Olympos ecotype, all measured parameters (root, cortex, stele areas, and stele/cortex ratio) were significantly reduced by NiO NP, especially at 500 mg/L of NiO NP (Fig. 3 A, B, C, D). According to data from the literature, 80% of Ni is stored in the vascular cylinder, which may reduce the diameter of the phloem and xylem (see, e.g., Page et al., 2006; dos Reis et al., 2017). On the contrary, the 250 mg/L exposure to NiO NP resulted in a significant increase in the ratio in the Loutra ecotype (Fig. 3 A, C, D). The areas of the stele and cortex increased as the effect of NiO NP exposure in Ampeliko root at 500 mg/L NiO NP (Fig. 3 B) resulted in an enhancement of the root area (Fig. 3 A).

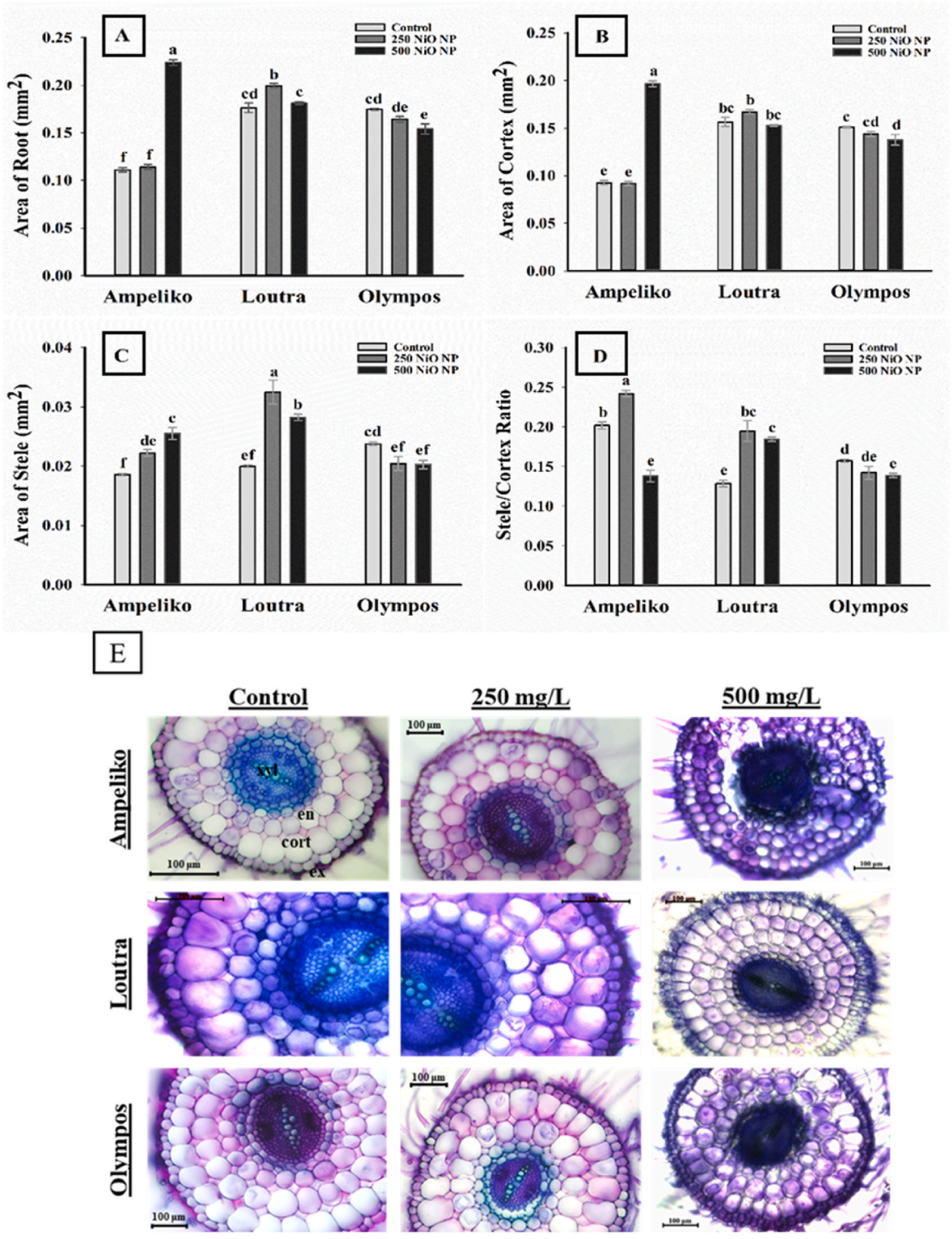

Fig. 3. Root area (A), cortex area (B), stele area (C) and stele/cortex ratio (D) measured in cross sections of primary roots of *Odontarrhena lesbiaca* (Ampeliko, Loutra and Olympos ecotypes) grown in the presence of 0, 250 or 500 mg/L NiO NP. Different letters indicate significant differences according to Duncan's test (n = 10, $P < 0.05$). (E) Representative cross sections of *O. lesbiaca* roots stained with toluidine blue. Scale bars = 100 µm. (For interpretation of the references to colour in this figure legend, the reader is referred to the Web version of this article.)

In Ampeliko root, at 0 and 250 mg/L of NiO NP concentration the cortex had two cell layers, while at 500 mg/L of NiO NP three cell layers could be detected (Fig. 3 E). An increased cortex thickness may support tolerance during Ni overload since it may provide resistance to radial water flow and thus reduce heavy metal transport (Pandey et al., 2022). The increment of the root area in Ampeliko and Loutra assumes cell wall thickening as a result of exposure to NiO NP.

Pectin levels in the root tissues of *Odontarrhena* ecotypes were differently affected by NiO NP treatments. In the mature zone of Ampeliko root, the pink colour associated with pectin slightly decreased as the effect of NiO NPs (indicated by arrows in Fig. 4 A) while in Loutra and Olympos, the pectin level increased in the root cap and root apical meristem or in the mature root zone, respectively (indicated by arrows in Fig. 4 A). Accumulation of pectic substances in the cell wall of Loutra and Olympos ecotype may result in more efficient Ni^{2+} binding due to the replacement of bounded Ca^{2+} (Dronnet et al., 1996; Krzesłowska, 2011; Loix et al., 2017). Based on this, we can assume that NiO NP-induced increase of pectin content in Odontarrhena roots may result in Ni^{2+} binding in the cell wall and consequently its exclusion from the cytoplasm.

Furthermore, lignin and suberin were detected simultaneously in root cross sections by Auramie-O (Fig. 4 B). In the untreated Ampeliko ecotype, fluorescence was visible in both the outer and inner tangential cell walls of the epidermis/exodermis, indicating the presence of suberin and the formation of the exodermis. In the endodermis, there was a tertiary endodermis with U-shaped secondary cell wall thickening due to suberin, along with an increasing amount of lignin deposition (Zeier et al., 1999). In the three ecotypes, both doses of NiO NP caused an increased fluorescence intensity in the tangential and radial cell walls of exodermal cells compared to the control (Fig. 4 B), indicating the formation of an exodermal suberin layer, which possibly acts as an outer barrier and delays metal ion or metal nanoparticle uptake (Cheng et al., 2014). Previously, increased lignin/suberin deposition in the exodermis was observed in the presence of heavy metals (Cheng et al., 2010, 2012) and a positive correlation was found between exodermal suberin formation and metal tolerance in mangrove species (Cheng et al., 2014).

3.6. Ecotype-dependent response of biomass production to NiO NP

The control individuals of the Olympos seedlings were significantly smaller than Ampeliko and Loutra, as indicated by most of the biomass parameters measured (Fig. 5). Regarding the effects of NP, the primary root length, the length of the shoot, the fresh weights of the root, the dry weight and the fresh weight of the shoot of Loutra were not significantly modified either by 250 or 500 mg/L of NiO NP. In case of Ampeliko, most of the measured biomass parameters were unmodified by the applied doses of NiO NP, with the exception of root length and fresh weight, where 250 mg/L of NiO NP caused a significant decrease compared to untreated plants (Fig. 5 A, B). On the contrary, all biomass parameters of Olympos seedlings were dose-dependently increased as a result of NiO NP effect (Fig. 5). For example, 250 mg/L NiO NP resulted in a 1.80-fold increase in root length, while 500 mg/L led to a 2.69-fold increase compared to the control (Fig. 5 A). It is fulfilled for all parameters that in the presence of NiO NP Olympos reached the size of control individuals of Ampeliko and Loutra (Fig. 5 A, B, D, E). The growth status of representative individuals of the *O. lesbiaca* ecotypes is illustrated in Fig. 5 G.

Using ionic Ni in the form of $NiCl_2$ in the same concentration and duration as the nanoform caused a significant decrease in the length of the Ampeliko shoot, did not affect the other parameters and slightly increased the dry weight of the root (at 250 mg/L dose, Fig. 6). On the contrary, in the case of Loutra, root length, shoot fresh and dry weight decreased in the presence of both $NiCl_2$ concentrations (Fig. 6 A, D, E). Interestingly, $NiCl_2$ did not cause any changes in Olympos growth and biomass parameters compared to the inducing effect of the same concentrations of NiO NP (Fig. 5). Presumably, the lower Ni ion concentrations released from NiO NPs were in the inducing range, while the higher Ni ion doses derived from NiCl2 were no longer induced but did not yet reduce biomass.

These implicate that the free salt form of Ni exerts more negative

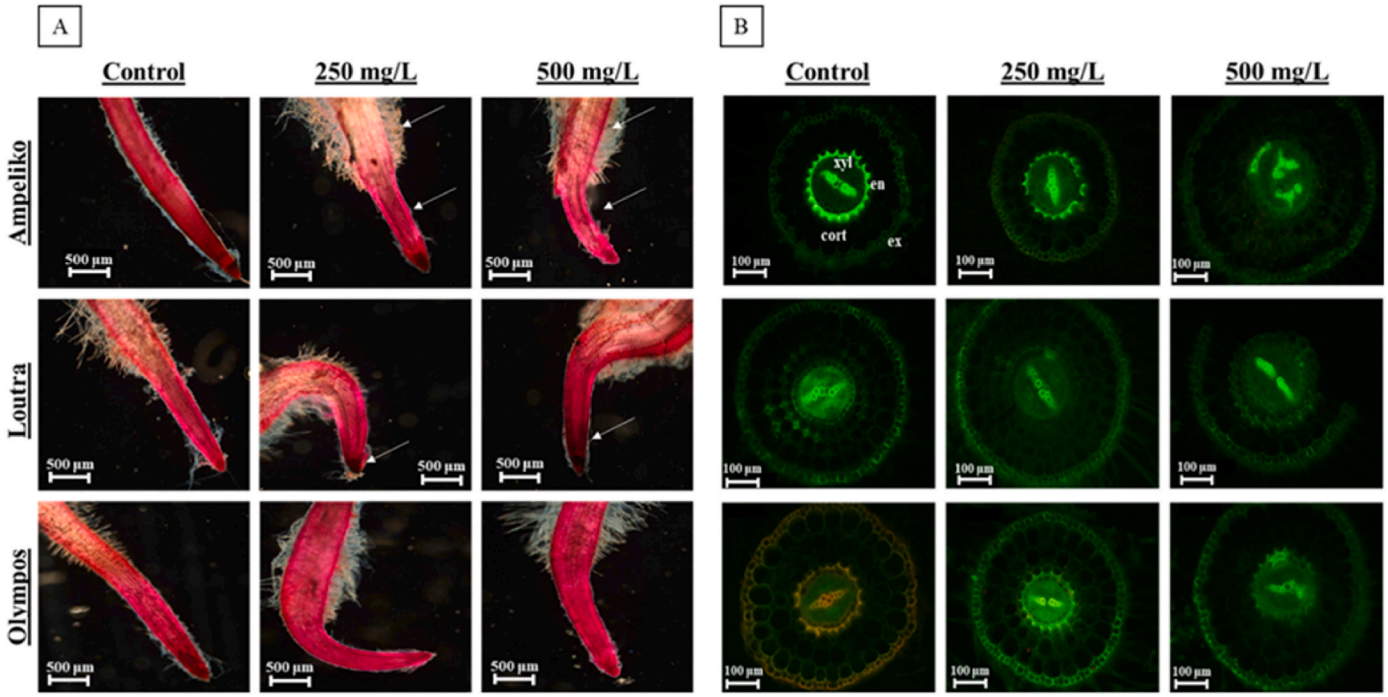

Fig. 4. (A) Pectin levels in the root tips of the *Odontarrhena lesbiaca* Ampeliko, Loutra, and Olympos ecotypes grown in the presence of 0 (control), 250 or 500 mg/L NiO NP for 5 days. Roots were labelled with ruthenium red (see Materials and Methods). Arrows indicate areas of increased or decreased staining compared to control. Scale bars = 500 µm. (B) Lignin/suberin levels in cross-sections of *O. lesbiaca* ecotypes. Root samples were labelled with Auramine-O (see Materials and Methods). Scale bars = 100 µm. (For interpretation of the references to colour in this figure legend, the reader is referred to the Web version of this article.)

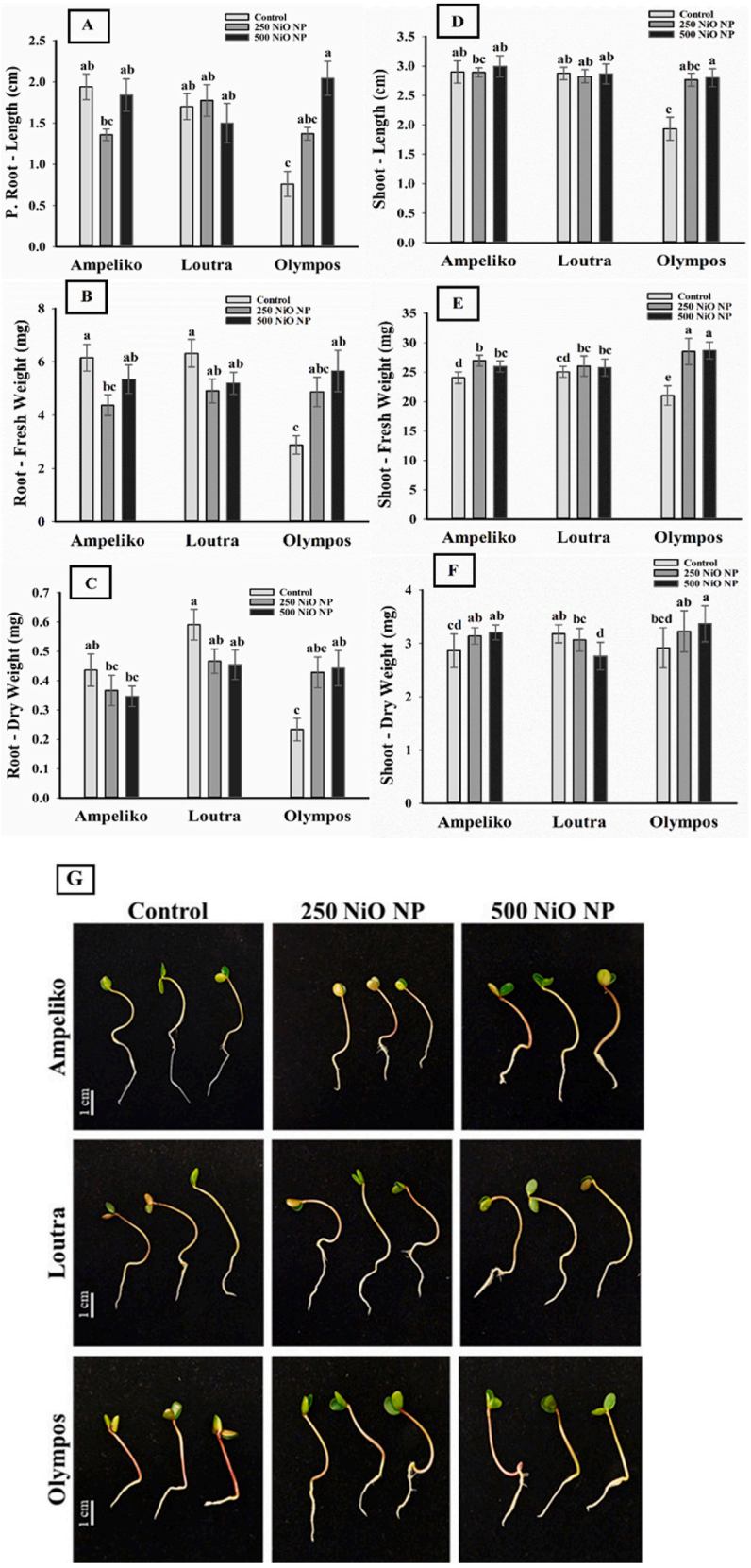

Fig. 5. Primary root length (A), fresh root weight (B), dry root weight (C), shoot length (D), fresh shoot weight (E) and dry shoot weight (F) of 5 days old *Odontarrhena lesciaca* seedlings germinated in the presence of 0 mg/L (control), 250 mg/L or 500 mg/L NiO NP. Different letters indicate significant differences according to Duncan's test (n = 10, $P < 0.05$). (G) Growth status of the control and NiO NP-exposed *O. lesbiaca* ecotypes (three seedlings/treatment). Scale bars = 1 cm.

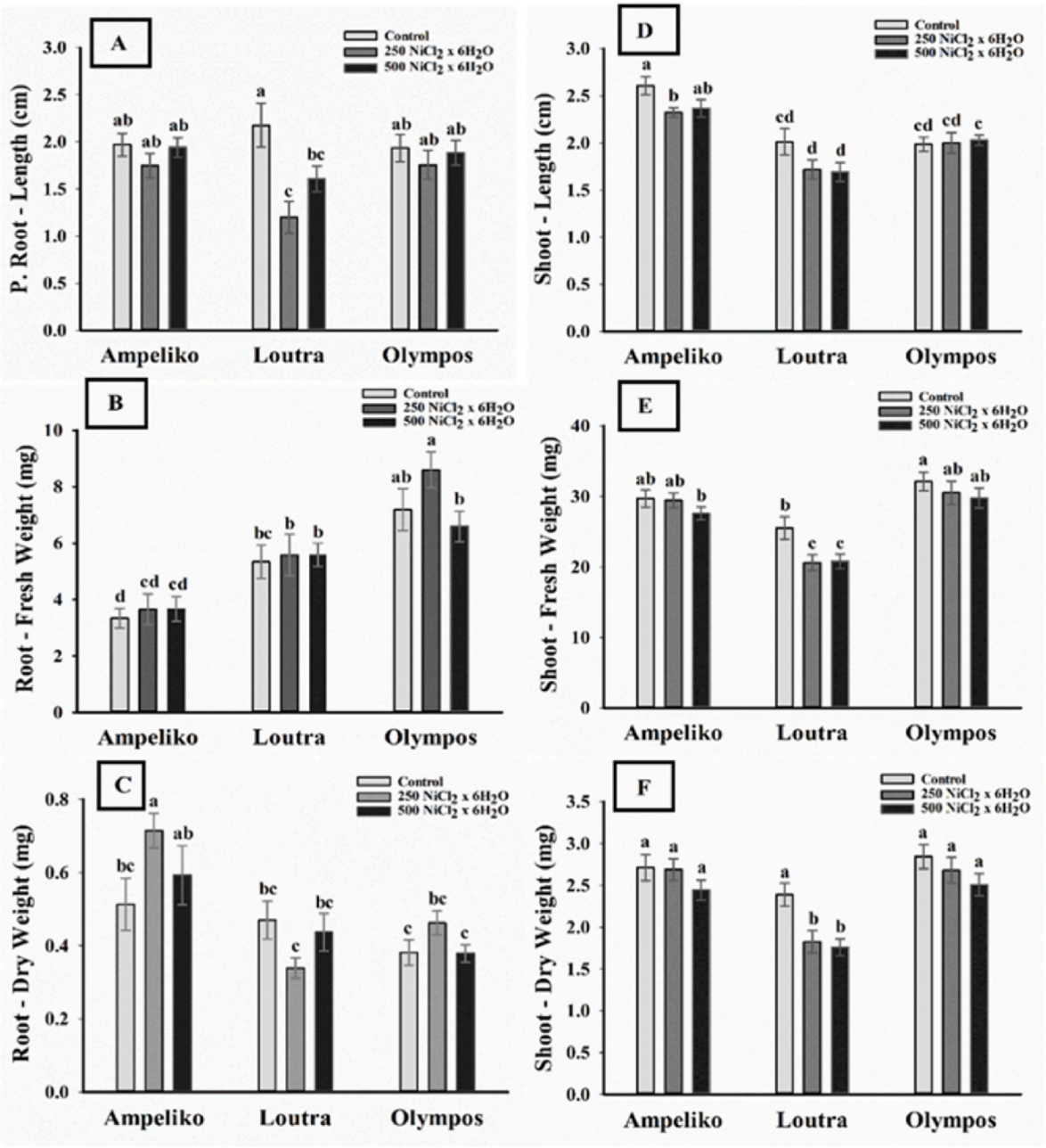

Fig. 6. Primary root length (A), fresh root weight (B), dry root weight (C), shoot length (D), fresh shoot weight (E) and dry shoot weight (F) of 5 days old *Odontarrhena lesciaca* seedlings germinated in the presence of 0 mg/L (control), 250 mg/L or 500 mg/L $NiCl_2 \times 6H_2O$. Different letters indicate significant differences according to Duncan's test (n = 10, $P < 0.05$).

effects compared to the nanoform possibly due to the higher levels of Ni ion released (Table 1). The results also indicate that the observed effects of nanoNiO can be attributed to the release of Ni ions.

3.7. NiO NPs trigger nitro-oxidative signalling in Odontarrhena lesbiaca seedlings

The production of NO was significantly induced by 250 mg/L of NiO NP in the roots of the Ampeliko and Loutra ecotypes, but it was unchanged in the roots of the Olympos ecotype (Fig. 7 A). Treatment with a concentration of 250 mg/L NiO NP resulted in a 26% increase in NO levels in Ampeliko and a 20% increase in Loutra compared to the control, while the double dose of NiO NP caused NO levels similar to control. Additionally, in the roots of the Olympos ecotype significant changes in NO levels were induced by neither NiO NP concentrations (Fig. 7 A). In our previous work, $NiCl_2$-induced NO formation was observed in the rhizotron-grown Ampeliko ecotype (Feigl et al., 2020) and in wild type *Arabidopsis thaliana* grown on agar (Kolbert et al., 2020). Similarly, NO levels were induced by increasing NiO NP dosages in *Allium cepa* roots, where NiO NPs induced the activation of nitrate reductase and nitric oxide synthase-like (NOS-like) enzymes suggesting their involvement in NP-induced increase in NO level (Manna et al., 2021). However, it must be noted that neither the coding gene nor the protein of the 'NOS-like enzyme' is known in higher plants (Jeandroz et al., 2016). The NiO NP treatment caused a concentration-dependent increase in $ONOO^-$ levels in the roots of Loutra and Olympos compared to the control (Fig. 7 B). In the case of Olympos, the 250 and 500 mg/L NiO NP-induced $ONOO^-$ accumulations were 20.7% and 35.6% compared to the control, respectively. Interestingly, no changes in $ONOO^-$ levels were caused by the presence of NiO NP in the Ampeliko

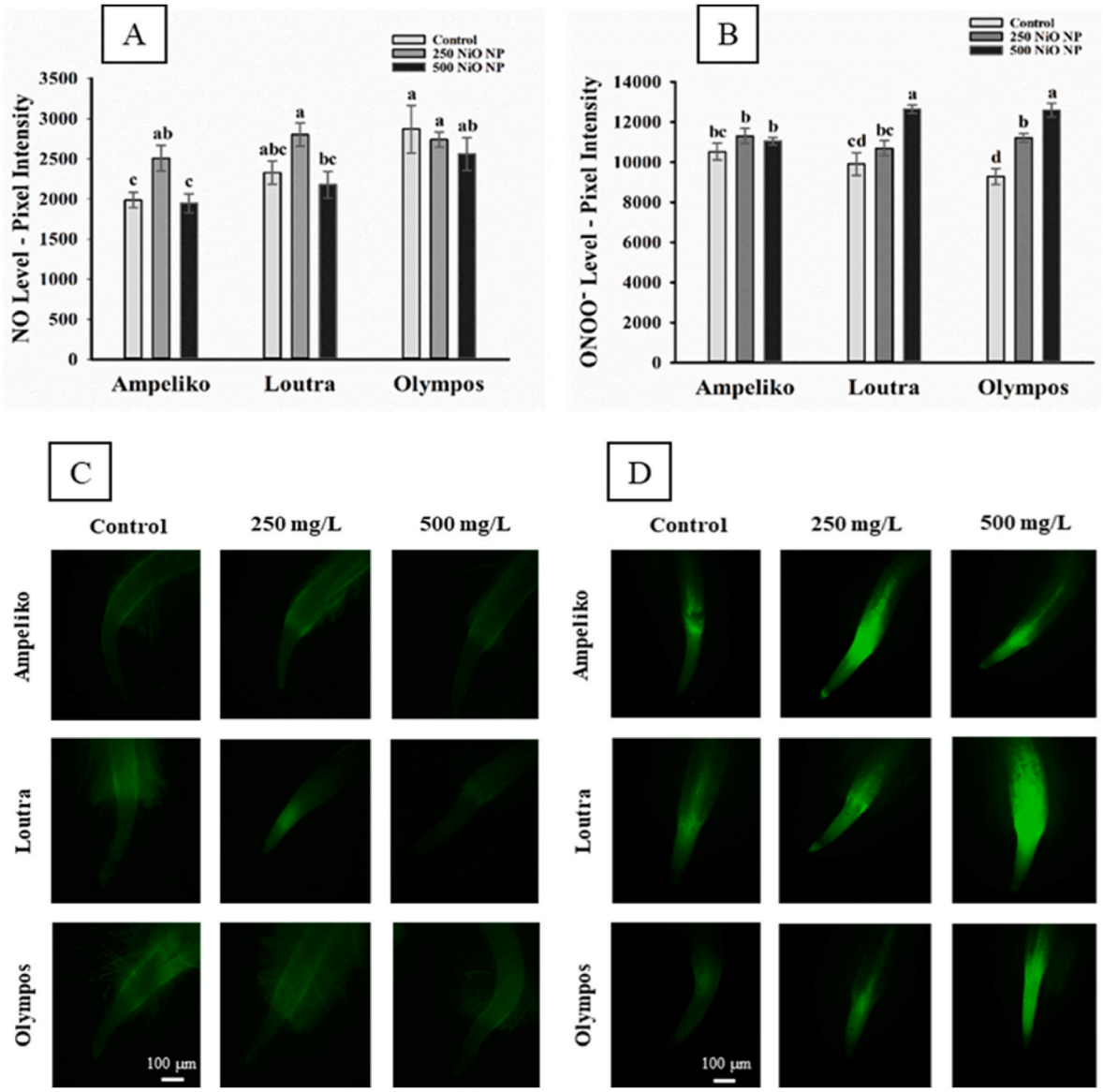

Fig. 7. The levels of nitric oxide (NO, A) and peroxynitrite ($ONOO^-$, B) (expressed as pixel intensities) in the root tips of the Ampeliko, Loutra, and Olympos ecotypes of *Odontarrhena lesbiaca* seedlings grown in the presence of 0, 250 mg/L or 500 mg/L NiO NP. Different letters indicate significant differences according to Duncan's test ($n = 10$, $P < 0.05$). Representative images showing root tips labelled with DAF-FM DA (C) or DHR123 (D) probes. Scale bars = 100 µm.

roots (Fig. 7 B).

Exposure to NiO NP caused a concentration-dependent decrease in GSNOR protein amount in Ampeliko roots, while in Loutra a significant decrease was caused only by the dose of NiO NP 500 mg/L. On the contrary, the amount of GSNOR increased significantly by 500 mg/L NiO NPs in the Olympos ecotype (Fig. 8 A, Fig. S3 A). Furthermore, in the shoot of the Loutra ecotype an obvious nanoNiO-induced increase in the amount of GSNOR protein was observed, while the Ampeliko and Olympos ecotypes showed reduced abundance of GSNOR proteins in the presence of both NiO NP concentrations (Fig. 8 B, Fig. S3 B). The effect of NiO on the amount of GSNOR protein shows an interesting opposite pattern in the shoot and root, suggesting that the effect of NiO NPs on the metabolism of the GSNOR protein is organ dependent.

Despite NiO NP-induced changes in protein amounts, no significant differences in enzyme activity were observed in the shoot due to the relatively large deviation of the data (Fig. 8 D). In the root, treatment with NiO NP 250 mg/L resulted in a decrease in GSNOR activity in Ampeliko, and both levels of NP exposure notably reduced GSNOR activity in Olympos (49% decrease by 250 mg/L and 31.5% decrease by 500 mg/L, Fig. 8 C). On the contrary, in Loutra, 250 mg/L of NiO NP caused a 77% increase, while treatment with 500 mg/L of NiO NP resulted in a 39.6% increase in GSNOR activity compared to control. In the root of the Loutra ecotype exposed to NiO NP, the reduced abundance of GSNOR proteins (Fig. 8 A) was accompanied by increased activity, suggesting a smaller but activated protein pool and implies the possibility of post-translational regulation of GSNOR in the presence of NiO NPs. In Olympos roots, an increase in protein abundance (Fig. 8 A) and an inhibition of activity was observed in the presence of NiO NP, which implies post-translational inhibition of GSNOR. Recent studies suggest that GSNOR activity may be post-translationally regulated by NADPH oxidase/respiratory burst oxidase homolog-mediated calcium and redox signals (Zhang et al., 2020; Chae et al., 2021; Li et al., 2021; Song et al., 2022) which may be a possible pathway of GSNOR regulation in this system.

3.8. Protein tyrosine nitration is positively correlated with Ni tolerance

Both organs of all three ecotypes show a basal nitration pattern

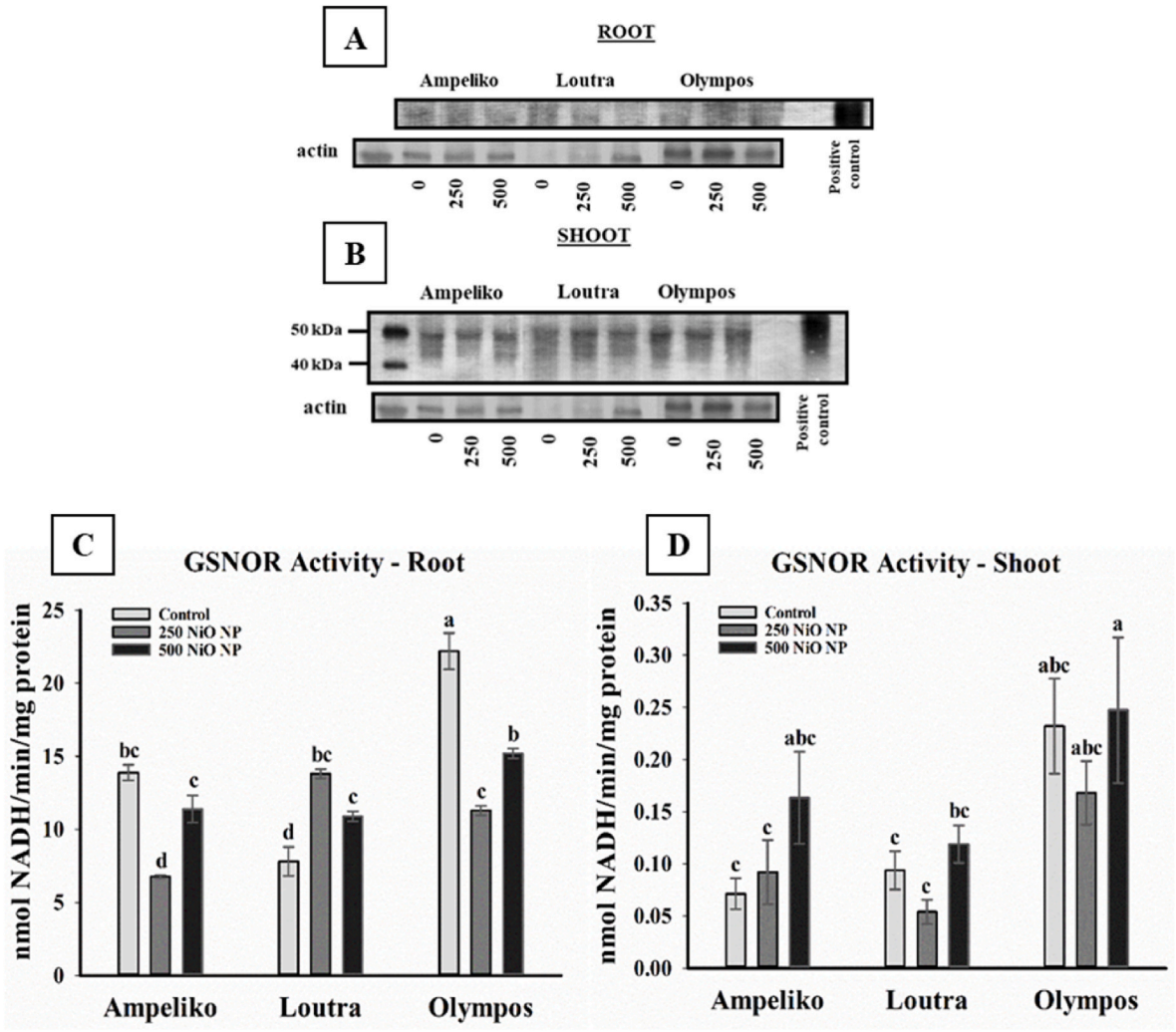

Fig. 8. Abundance of GSNOR protein in the root (A) and shoot (B) of *Odontarrhena lesbiaca* ecotypes (Ampeliko, Loutra, Olympos) exposed to 0, 250 or 500 mg/L of NiO NP. Activity of GSNOR (expressed as nmol NADH/min/mg protein) in the root (C) and shoot (D) of NiO NP-treated *O. lesbiaca* seedlings. Different letters indicate significant differences according to Duncan's test (n = 5, $P < 0.05$).

indicating a physiological pool of nitrated proteins similarly to other plant species (reviewed in Kolbert et al., 2017; Corpas et al., 2021). In Ampeliko roots, the level of protein tyrosine nitration slightly increased in at least seven bands and in Loutra in at least four bands upon NiO NP exposure. In Olympos roots, signal intensity related to tyrosine nitration increased in one and decreased in two bands (Fig. 9 A, Fig. S4). A decrease in the nitration signal assumes the activation of defense processes due to proteasomal degradation of nitrated proteins. However, there is little solid evidence for proteasomal elimination of nitrated proteins in plants (Kolbert et al., 2017).

In the shoot, the application of NiO NPs led to a small increase in protein nitration in Ampeliko in at least four bands and in Loutra in at least three bands (Fig. 9 B, Fig. S4). However, in Loutra, the signal decreased in one protein band, and in Olympos, it decreased in two bands. In Olympos, there was a small increase in two protein bands. Taken together, the NiO NP-induced enhancement in physiological protein nitration is slight in all three ecotypes, possibly due to the Ni hyperaccumulator/tolerant character of this species. The high dose of $NiCl_2$ exposure (3000 mg/kg) caused a similar moderate increase in protein nitration in the Ampeliko and Loutra ecotypes (Feigl et al., 2020). Minor variations among ecotypes were observed as the shoot and root of Olympos seedlings exhibited a reduced number of protein bands with intensified nitration compared to Ampeliko and Loutra. The dissimilarities in the level of protein nitration induced by NiO NPs correlate with the biomass production of the ecotypes, indicating that Ampeliko is the most susceptible, Loutra displays moderate sensitivity, and Olympos exhibits the highest tolerance to NiO NP exposure.

4. Conclusions

All three ecotypes show the characteristics of Ni hyperaccumulators due to their high basal Ni content, efficient root-to-shoot translocation, and consequently high Ni tissue concentrations in the shoot. The Ni translocation has a lower rate in the case of NiO NP treatment compared to $NiCl_2$, possibly due to the binding of the NPs to the root cell wall. The observed increase in the pectin level of the roots potentiates Ni^{2+} binding in the root cell walls. The effect of NiO NP on seedling development depends on the ecotype, and the results also indicate that the observed effects of nanoNiO can be attributed to the release of Ni ions. Exposure to NiO NP induces the production of NO and $ONOO^-$, and putatively regulates GSNOR at the post-translational level. Tyrosine nitration increases with the effect of NiO NPs, and the rate of this protein modification is in accordance with changes in the biomass production of Ni hyperaccumulators.

Overall, our results demonstrate for the first time that the tolerance of *Odontarrhena lesbiaca* ecotypes against NiO NPs manifests at cellular (binding of NPs by the root cell wall due to compositional modification), tissue (root anatomical changes), organ/organism (slight modifications

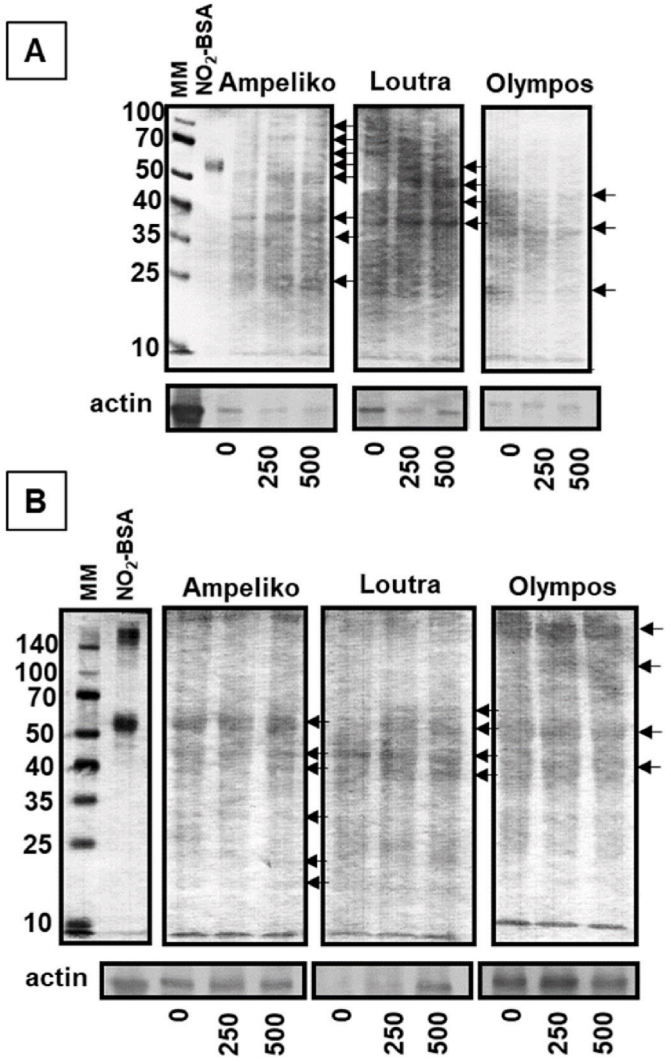

Fig. 9. Representative Western blot membranes showing tyrosine protein nitration in root (A) and shoot (B) of the *Odontarrhena lesbiaca* ecotypes (Ampeliko, Loutra, Olympos) exposed to 0, 250 or 500 mg/L NiO NP. MM = molecule marker, NO_2-BSA = nitrated bovine serum albumin. The black arrows indicate protein bands with altered signal intensity.

in biomass production) and molecular (changes in RNS metabolism and induced nitrosative protein modification) levels.

Declaration of competing interest

The authors declare that they have no known competing financial interests or personal relationships that could have appeared to influence the work reported in this paper.

Data availability

Data will be made available on request.

Acknowledgements

This work was supported by the National Research, Development and Innovation Office of Hungary under grant No. K 135303 (Zs.K.), K 129063 (G.G.) and TKP2021-NVA-19 (G.G.).

Authors are grateful to Zsolt Rázga† for his valuable contribution to TEM analysis. Authors would like to thank to Éva Kapásné Török for her valuable help during the experiments. The skillful help of Fernando A. Casian Plaza (University of Szeged) in the preparation of the LIBS elemental maps is highly appreciated.

Appendix A. Supplementary data

Supplementary data to this article can be found online at https://doi.org/10.1016/j.envpol.2023.122874.

References

Adamidis, G.C., Aloupi, M., Kazakou, E., Dimitrakopoulos, P.G., 2014. Intra-specific variation in Ni tolerance, accumulation and translocation patterns in the Ni-hyperaccumulator *Alyssum lesbiacum*. Chemosphere 95, 496–502. https://doi.org/10.1016/j.chemosphere.2013.09.106.

Barroso, J.B., Corpas, F.J., Carreras, A., Rodríguez-Serrano, M., Esteban, F.J., Fernandez-Ocana, A., 2006. Localization of *S*-nitrosoglutathione and expression of *S*-nitrosoglutathione reductase in pea plants under cadmium stress. J. Exp. Bot. 57, 1785–1793. https://doi.org/10.1093/jxb/erj175.

Bhat, J.A., Basit, F., Alyemeni, M.N., Mansoor, S., Kaya, C., Ahmad, P., 2023. Gibberellic acid mitigates nickel stress in soybean by cell wall fixation and regulating oxidative stress metabolism and glyoxalase system. Plant Physiol. Biochem. 198, 107678 https://doi.org/10.1016/j.plaphy.2023.107678.

Bradford, M.M., 1976. A rapid and sensitive method for the quantitation of microgram quantities of protein utilizing the principle of protein-dye binding. Anal. Biochem. 72, 248–254. https://doi.org/10.1016/0003-2697(76)90527-3.

Chae, H.B., Kim, M.G., Kang, C.H., Park, J.H., Lee, E.S., Lee, S.U., et al., 2021. Redox sensor QSOX1 regulates plant immunity by targeting GSNOR to modulate ROS generation. Mol. Plant 14 (8), 1312–1327. https://doi.org/10.1016/j.molp.2021.05.004.

Cheng, H., Liu, Y., Tam, N.F.Y., Wang, X., Li, S.Y., Chen, G.Z., Ye, Z.H., 2010. The role of radial oxygen loss and root anatomy on zinc uptake and tolerance in mangrove seedlings. Environ. Pollut. 158 (5), 1189–1196. https://doi.org/10.1016/j.envpol.2010.01.025.

Cheng, H., Tam, N.F.Y., Wang, Y., Li, S., Chen, G., Ye, Z., 2012. Effects of copper on growth, radial oxygen loss and root permeability of seedlings of the mangroves *Bruguiera gymnorrhiza* and *Rhizophora stylosa*. Plant Soil 359, 255–266. https://doi.org/10.1007/s11104-012-1171-1.

Cheng, H., Jiang, Z.Y., Liu, Y., Ye, Z.H., Wu, M.L., Sun, C.C., et al., 2014. Metal (Pb, Zn and Cu) uptake and tolerance by mangroves in relation to root anatomy and lignification/suberization. Tree Physiol. 34 (6), 646–656. https://doi.org/10.1093/treephys/tpu042.

Corpas, F.J., González-Gordo, S., Palma, J.M., 2021. Protein nitration: a connecting bridge between nitric oxide (NO) and plant stress. Plant Stress 2, 100026. https://doi.org/10.1016/j.stress.2021.100026.

Danjumma, S.G., Abubakar, Y., Suleiman, S., 2019. Nickel oxide (NiO) devices and applications: a review. J. Eng. Res. Technol. 8, 12–21. https://doi.org/10.17577/IJERTV8IS040281.

dos Reis, A.R., de Queiroz Barcelos, J.P., de Souza Osório, C.R.W., Santos, E.F., Lisboa, L. A.M., Santini, J.M.K., Gratao, P.L., 2017. A glimpse into the physiological, biochemical and nutritional status of soybean plants under Ni-stress conditions. Environ. Exp. Bot. 144, 76–87. https://doi.org/10.1016/j.envexpbot.2017.10.006.

Dronnet, V.M., Renard, C.M.G.C., Axelos, M.A.V., Thibault, J.F., 1996. Heavy metals binding by pectins: selectivity, quantification and characterization. Biotechnol. Prog. 14, 535–540. https://doi.org/10.1016/S0921-0423(96)80283-8.

Durand, C., Vicré-Gibouin, M., Follet-Gueye, M.L., Duponchel, L., Moreau, M., Lerouge, P., Driouich, A., 2009. The organization pattern of root border-like cells of Arabidopsis is dependent on cell wall homogalacturonan. Plant Physiol. 150 (3), 1411–1421. https://doi.org/10.1104/pp.109.136382.

Fabiano, C.C., Tezotto, T., Favarin, J.L., Polacco, J.C., Mazzafera, P., 2015. Essentiality of nickel in plants: a role in plant stresses. Front. Plant Sci. 6, 754. https://doi.org/10.3389/fpls.2015.00754.

Feigl, G., Varga, V., Molnár, Á., Dimitrakopoulos, P.G., Kolbert, Z., 2020. Different nitro-oxidative response of *Odontarrhena lesbiaca* plants from geographically separated habitats to excess nickel. Antioxidants 9 (9), 837. https://doi.org/10.3390/antiox9090837.

Gajewska, E., Skłodowska, M., Słaba, M., Mazur, J., 2006. Effect of nickel on antioxidative enzyme activities, proline and chlorophyll contents in wheat shoots. Biol. Plant. (Prague) 50, 653–659. https://doi.org/10.1007/s10535-006-0102-5.

Galbács, G. (Ed.), 2022. Laser-induced Breakdown Spectroscopy in Biological, Forensic and Materials Sciences. Springer. ISBN978-3-031-14501-8.

Galetskiy, D., Lohscheider, J., Kononikhin, A., Popov, I., Nikolaev, E., Adamska, I., 2011. Phosphorylation and nitration levels of photosynthetic proteins are conversely regulated by light stress. Plant Mol. Biol. 77, 461–473. https://doi.org/10.1007/s11103-011-9824-7.

Genchi, G., Carocci, A., Lauria, G., Sinicropi, M.S., Catalano, A., 2020. Nickel: human health and environmental toxicology. Int. J. Environ. Res. Publ. Health 17 (3), 679.

Halliwell, B., Gutteridge, J., 1984. Oxygen toxicity, oxygen radicals, transition metals and disease. Biochem. J. 219 (1), 1–14. https://doi.org/10.1042/bj2190001.

Hipfinger, C., Laux, M., Puschenreiter, M., 2022. Comparison of four nickel hyperaccumulator species in the temperate climate zone of Central Europe. J. Geochem. Explor. 234, 106933 https://doi.org/10.1016/j.gexplo.2021.106933.

Hseu, Z.Y., Chen, Z.S., 2019. Nickel in Serpentine Soils. Nickel in Soils and Plants. CRC Press. https://doi.org/10.1201/9781315154664. Chapter 8, eBook ISBN 9781315154664.

Hussain, M.B., Ali, S., Azam, A., Hina, S., Farooq, M.A., Ali, B., et al., 2013. Morphological, physiological and biochemical responses of plants to nickel stress: a review. Afr. J. Agric. Res. 8 (17), 1596–1602. https://doi.org/10.5897/AJAR12.407.

Ingle, R.A., Mugford, S.T., Rees, J.D., Campbell, M.M., Smith, J.A.C., 2005. Constitutively high expression of the histidine biosynthetic pathway contributes to nickel tolerance in hyperaccumulator plants. Plant Cell 17 (7), 2089–2106. https://doi.org/10.1105/tpc.104.030577.

Jahnová, J., Luhová, L., Petřivalský, M., 2019. S-nitrosoglutathione reductase—the master regulator of protein S-nitrosation in plant NO signaling. Plants 8 (2), 48. https://doi.org/10.3390/plants8020048.

Janovszky, P., Kéri, A., Palásti, D.J., Brunnbauer, L., Domoki, F., Limbeck, A., Galbács, G., 2023. Quantitative elemental mapping of biological tissues by laser-induced breakdown spectroscopy using matrix recognition. Sci. Rep. 13, 10089 https://doi.org/10.1038/s41598-023-37258-y.

Jeandroz, S., Wipf, D., Stuehr, D.J., Lamattina, L., Melkonian, M., Tian, Z., Wendehenne, D., 2016. Occurrence, structure, and evolution of nitric oxide synthase–like proteins in the plant kingdom. Sci. Signal. 9 (417) https://doi.org/10.1126/scisignal.aad4403 re2-re2.

Kazakou, E., Adamidis, G.C., Baker, A.J.M., Reeves, R.D., Godino, M., Dimitrakopoulos, P.G., 2010. Species adaptation in serpentine soils in Lesbos Island (Greece): metal hyperaccumulation and tolerance. Plant Soil 332, 369–385. https://doi.org/10.1007/s11104-010-0302-9.

Khair, K.U., Farid, M., Ashraf, U., Zubair, M., Rizwan, M., Farid, S., et al., 2020. Citric acid enhanced phytoextraction of nickel (Ni) and alleviate *Mentha piperita* (L.) from Ni-induced physiological and biochemical damages. Environ. Sci. Pollut. Res. 27, 27010–27022. https://doi.org/10.1007/s11356-020-08978-9.

Khaliq, A., Ali, S., Hameed, A., Farooq, M.A., Farid, M., Shakoor, M.B., Rizwan, M., 2015. Silicon alleviates nickel toxicity in cotton seedlings through enhancing growth, photosynthesis, and suppressing Ni uptake and oxidative stress. Arch. Agron Soil Sci. 62 (5), 633–647. https://doi.org/10.1080/03650340.2015.1073263.

Kolbert, Z., Andrea, P., Nóra, L., Feigl, G., Ördög, A., Erdei, L., 2012. *In vivo* and *in vitro* studies on fluorophore-specificity. Acta Biol. Szeged. 56 (1), 37–41.

Kolbert, Z., Feigl, G., Bordé, Á., Molnár, Á., Erdei, L., 2017. Protein tyrosine nitration in plants: present knowledge, computational prediction and future perspectives. Plant Physiol. Biochem. 113, 56–63. https://doi.org/10.1016/j.plaphy.2017.01.028.

Kolbert, Z., Molnár, Á., Szőllősi, R., Feigl, G., Erdei, L., Ördög, A., 2018. Nitro-oxidative stress correlates with Se tolerance of *Astragalus* species. Plant Cell Physiol. 59 (9), 1827–1843. https://doi.org/10.1093/pcp/pcy099.

Kolbert, Z., Oláh, D., Molnár, Á., Szőllősi, R., Erdei, L., Ördög, A., 2020. Distinct redox signalling and nickel tolerance in *Brassica juncea* and *Arabidopsis thaliana*. Ecotoxicol. Environ. Saf. 189, 109989 https://doi.org/10.1016/j.ecoenv.2019.109989.

Kolbert, Z., Szőllősi, R., Rónavári, A., Molnár, Á., 2022. Nanoforms of essential metals: from hormetic phytoeffects to agricultural potential. J. Exp. Bot. 73 (6), 1825–1840. https://doi.org/10.1093/jxb/erab547.

Kruckeberg, A.R., 2002. The influences of lithology on plant life. In: Geology and Plant Life: the Effects of Landforms and Rock Type on Plants. University of Washington Press, Seattle, WA, USA, pp. 160–181.

Krzesłowska, M., 2011. The cell wall in plant cell response to trace metals: polysaccharide remodeling and its role in defense strategy. Acta Physiol. Plant. 33, 35–51. https://doi.org/10.1007/s11738-010-0581-z.

Kumar, S., Wang, M., Liu, Y., Fahad, S., Qayyum, A., Jadoon, S.A., Zhu, G., 2022. Nickel toxicity alters growth patterns and induces oxidative stress response in sweetpotato. Front. Plant Sci. 13 https://doi.org/10.3389/fpls.2022.1054924.

Kurczyńska, E., Godel-Jędrychowska, K., Sala, K., Milewska-Hendel, A., 2021. Nanoparticles—plant interaction: what we know, where we are? Appl. Sci. 11 (12), 5473. https://doi.org/10.3390/app11125473.

Li, B., Sun, C., Lin, X., Busch, W., 2021. The emerging role of GSNOR in oxidative stress regulation. Trends Plant Sci. 26 (2), 156–168. https://doi.org/10.1016/j.tplants.2020.09.004.

Limbeck, A., Brunnbauer, L., Lohninger, H., Porízka, P., Modlitbova, P., Kaiser, J., Janovszky, P., Kéri, A., Galbács, G., 2021. Methodology and applications of elemental mapping by laser induced breakdown spectroscopy. Anal. Chim. Acta 1147, 72–98. https://doi.org/10.1016/j.aca.2020.12.054.

Lin, D., Xing, B., 2007. Phytotoxicity of nanoparticles: inhibition of seed germination and root growth. Environ. Pollut. 150 (2), 243–250. https://doi.org/10.1016/j.envpol.2007.01.016.

Loix, C., Huybrechts, M., Vangronsveld, J., Gielen, M., Keunen, E., Cuypers, A., 2017. Reciprocal interactions between cadmium-induced cell wall responses and oxidative stress in plants. Front. Plant Sci. 8, 1867. https://doi.org/10.3389/fpls.2017.01867.

Manna, I., Sahoo, S., Bandyopadhyay, M., 2021. Effect of engineered nickel oxide nanoparticle on reactive oxygen species–nitric oxide interplay in the roots of *Allium cepa* L. Front. Plant Sci. 12, 586509 https://doi.org/10.3389/fpls.2021.586509.

Manna, I., Mishra, S., Bandyopadhyay, M., 2022. In vivo genotoxicity assessment of nickel oxide nanoparticles in the model plant *Allium cepa* L. Nucleus 65, 203–214. https://doi.org/10.1007/s13237-021-00377-w.

Mateos, D., Valdez, B., Castillo, J.R., Nedev, N., Curiel, M., Perez, O., Tiznado, H., 2019. Synthesis of high purity nickel oxide by a modified sol-gel method. Ceram. Int. 45 (9), 11403–11407. https://doi.org/10.1016/j.ceramint.2019.03.005.

Mitra, P.P., Loqué, D., 2014. Histochemical staining of *Arabidopsis thaliana* secondary cell wall elements. JoVE 87, e51381. https://doi.org/10.3791/51381.

Molassiotis, A., Fotopoulos, V., 2011. Oxidative and nitrosative signaling in plants: two branches in the same tree? Plant Signal. Behav. 6 (2), 210–214. https://doi.org/10.4161/psb.6.2.14878.

Molnár, Á., Rónavári, A., Bélteky, P., Szőllősi, R., Valyon, E., Oláh, D., Kolbert, Z., 2020. ZnO nanoparticles induce cell wall remodeling and modify ROS/RNS signalling in roots of *Brassica* seedlings. Ecotoxicol. Environ. Saf. 206, 111158 https://doi.org/10.1016/j.ecoenv.2020.111158.

Mustafa, A., Zulfiqar, U., Mumtaz, M.Z., Brtnicky, M., 2023. Nickel (Ni) phytotoxicity and detoxification mechanisms: a review. Chemosphere 328, 138574. https://doi.org/10.1016/j.chemosphere.2023.138574.

Oláh, D., Feigl, G., Molnár, Á., Ördög, A., Kolbert, Z., 2020. Strigolactones interact with nitric oxide in regulating root system architecture of *Arabidopsis thaliana*. Front. Plant Sci. 11, 1019. https://doi.org/10.3389/fpls.2020.01019.

Oliveira, H.C., Seabra, A.B., Kondak, S., Adedokun, O.P., Kolbert, Z., 2023. Multilevel approach to plant–nanomaterial relationships: from cells to living ecosystems. J. Exp. Bot. 74 (12), 3406–3424. https://doi.org/10.1093/jxb/erad107.

Page, V., Weisskopf, L., Feller, U., 2006. Heavy metals in white lupin: uptake, root-to-shoot transfer and redistribution within the plant. New Phytol. 171 (2), 329–341. https://doi.org/10.1111/j.1469-8137.2006.01756.x.

Pandey, A.K., Zorić, L., Sun, T., Karanović, D., Fang, P., Borišev, M., et al., 2022. The anatomical basis of heavy metal responses in legumes and their impact on plant–rhizosphere interactions. Plants 11 (19), 2554. https://doi.org/10.3390/plants11192554.

Rahoui, S., Martinez, Y., Sakouhi, L., Ben, C., Rickauer, M., Rickauer, M., Ferjani, E.E., Gentzbittel, L., Chaoui, A., 2017. Cadmium-induced changes in antioxidative systems and differentiation in roots of contrasted *Medicago truncatula* lines. Protoplasma 254, 473–489. https://doi.org/10.1007/s00709-016-0968-9.

Rascio, N., Navari-Izzo, F., 2011. Heavy metal hyperaccumulating plants: how and why do they do it? And what makes them so interesting? Plant Sci. 180 (2), 169–181. https://doi.org/10.1016/j.plantsci.2010.08.016.

Reeves, R.D., 1992. The hyperaccumulation of nickel by serpentine plants. In: Baker, A.J.M., Proctor, J., Reeves, R.D. (Eds.), The Vegetation of Ultramafic (Serpentine) Soils. Intercept Ltd, Andover, UK), pp. 253–277.

Reeves, R.D., Baker, A.J., Jaffré, T., Erskine, P.D., Echevarria, G., van Der Ent, A., 2017. A global database for plants that hyperaccumulate metal and metalloid trace elements. New Phytol. 218 (2), 407–411. https://doi.org/10.1111/nph.14907.

Reeves, R.D., van der Ent, A., Echevarria, G., Isnard, S., Baker, A.J.M., 2021. Global distribution and ecology of hyperaccumulator plants. In: van der Ent, A., Baker, A.J.M., Echevarria, G., Simonnot, M.O., Morel, J.L. (Eds.), Agromining: Farming for Metals; Mineral Resource Reviews. Springer, Cham, Switzerland, pp. 133–154. https://doi.org/10.1007/978-3-030-58904-2_7.

Saad, R., Kobaissi, A., Robin, C., Echevarria, G., Benizri, E., 2016. Nitrogen fixation and growth of *Lens culinaris* as affected by nickel availability: a pre-requisite for optimization of agromining. Environ. Exp. Bot. 131, 1–9. https://doi.org/10.1016/j.envexpbot.2016.06.010.

Sakamoto, A., Ueda, M., Morikawa, H., 2002. *Arabidopsis* glutathione-dependent formaldehyde dehydrogenase is an *S*-nitrosoglutathione reductase. FEBS (Fed. Eur. Biochem. Soc.) Lett. 515 (1–3), 20–24. https://doi.org/10.1016/S0014-5793(02)02414-6.

Shahzad, B., Tanveer, M., Rehman, A., Cheema, S.A., Fahad, S., Rehman, S., Sharma, A., 2018. Nickel; whether toxic or essential for plants and environment-A review. Plant Physiol. Biochem. 132, 641–651. https://doi.org/10.1016/j.plaphy.2018.10.014.

Shi, G., Cai, Q., 2009. Leaf plasticity in peanut (*Arachis hypogaea* L.) in response to heavy metal stress. Environ. Exp. Bot. 67 (1), 112–117. https://doi.org/10.1016/j.envexpbot.2009.02.009.

Song, X., Liu, J., Geng, N., Shan, Y., Zhang, B., Zhao, B., Zhang, Y., 2022. Multi-omics analysis to reveal disorders of cell metabolism and integrin signaling pathways induced by $PM_{2.5}$. J. Hazard Mater. 424, 127573 https://doi.org/10.1016/j.jhazmat.2021.127573. Part C).

Sreekanth, T.V.M., Nagajyothi, P.C., Lee, K.D., Prasad, T.N.V.K.V., 2013. Occurrence, physiological responses and toxicity of nickel in plants. Int. J. Environ. Sci. Technol. 10, 1129–1140. https://doi.org/10.1007/s13762-013-0245-9.

Stampoulis, D., Sinha, S.K., White, J.C., 2009. Assay-dependent phytotoxicity of nanoparticles to plants. Environ. Sci. Technol. 43 (24), 9473–9479. https://doi.org/10.1021/es901695c.

Strid, A., Tan, K., 2002. Flora Hellenica; A.R.G. Gantner Verlag K.G.: Ruggell, Liechtenstein 2.

Van der Pas, L., Ingle, R.A., 2019. Towards an understanding of the molecular basis of nickel hyperaccumulation in plants. Plants 8 (1), 11. https://doi.org/10.3390/plants8010011.

Wang, D., Xu, R., Wang, X., Li, Y., 2006. NiO nanorings and their unexpected catalytic property for CO oxidation. Nanotechnology 17 (4), 979. https://doi.org/10.1088/0957-4484/17/4/023.

Zeier, J., Goll, A., Yokoyama, M., Karahara, I., Schreiber, L., 1999. Structure and chemical composition of endodermal and rhizodermal/hypodermal walls of several species. Plant Cell Environ. 22 (3), 271–279. https://doi.org/10.1046/j.1365-3040.1999.00401.x.

Zelko, I., Lux, A., Sterckeman, T., Martinka, M., Kollárová, K., Lišková, D., 2012. An easy method for cutting and fluorescent staining of thin roots. Ann. Bot. 110 (2), 475–478. https://doi.org/10.1093/aob/mcs046.

Zhang, X., Wang, W., Kang, X., Zhao, L., 2020. Arabidopsis CaM3 inhibits nitric oxide accumulation and improves thermotolerance by promoting *S*-nitrosoglutathione reductase via direct binding. Plant Growth Regul. 90, 41–50. https://doi.org/10.1007/s10725-019-00552-9.